

Versatile surface functionalization of cyclic olefin copolymer (COC) with sputtered SiO₂ thin film for potential BioMEMS applications

Kuo-Sheng Ma, Faisal Reza, Ishtiaq Saaem and Jingdong Tian*

Department of Biomedical Engineering and the Institute for Genome Sciences and Policy, Duke University, 36 Hudson Hall, Box 90281, Durham, NC 27708-0281, USA. E-mail: jtian@duke.edu

Received 6th March 2009, Accepted 12th August 2009

First published on the web 9th September 2009

Cyclic olefin copolymer (COC) is a new class of thermoplastic polymers used for a variety of applications ranging from bio-sensing to optics. However, lack of functional groups and intense surface hydrophobicity hamper further development and application of this material. Here, we describe fabrication and characterization of SiO₂-COC hybrid material (oxCOC), which provides a desirable substrate for microfluidic devices and subsequent surface modifications. The deposited SiO₂ thin film on COC surface was characterized by X-ray photoelectron spectroscopy and Fourier transform infrared spectroscopy. The new SiO₂-COC hybrid was found to have similar high optical transmission properties as that of pristine COC. Profilometric and AFM analysis revealed no dramatic change in morphology or surface roughness of functionalized COC. The SiO₂-COC hybrid appeared to be stable in most of the solvents evaluated and could be further modified by other compounds, such as 3-aminopropyltriethoxy silane (APTES). The new SiO₂-COC hybrid material and the robust fabrication method are expected to enable a variety of BioMEMS applications.

1. Introduction

With emerging interest in novel materials for microfabrication, polymers have gained significant attention as promising materials for rapid prototyping. Various polymers with diverse properties provide practical, versatile and cost-effective alternatives to the inorganic substrates (*i.e.* silicon or glass) for micro-devices fabrication. Recently, a new class of thermoplastic polymer, cyclic olefin copolymer, has attracted special attention due to its desirable properties such as low auto-fluorescence, low density, low moisture adsorption, excellent optical and UV transparency, high stiffness, and resistance to organic solvents.¹ Products composed of COC exhibit a glass transition temperature (T_g) ranging from 70 °C to 180 °C.² COC has been utilized in micro-electrical-mechanical systems (MEMS)³⁻⁵ and micro total analysis systems (μTAS).⁶⁻⁸ Inexpensive and easily replicable fabrication techniques such as injection molding⁹ and hot embossing¹⁰ have been used extensively and successfully on COC.

For most microfluidic “lab-on-a-chip” bio-sensing and bio-analytical applications, it is desirable to have a hydrophilic surface with appropriate functional groups for biomolecular conjugation. However, like most commodity polymers used in microfabrications, COC presents a chemically inert and highly hydrophobic surface. The hydrophobic surface will create significant difficulties for liquid injection and flow control in microfluidic channels. The lack of functional surface groups for immobilizing biomolecules poses an additional hindrance for potential applications of COC in biomolecular recognition and analysis.

A number of methods have been developed to mitigate such problems. Photografting has been developed as a technique for surface modifications of synthetic polymers used for microfabrication. This technique has been extended for COC microfluidic device fabrication. Different types of monomers, such as acrylamide and methyl acrylate, have been successfully grafted on the surface of COC to generate various functional groups.^{9,11-13} The UV-initiated and benzophenone-mediated photografting process generates branched and cross-linked polymer architecture on the substrate surface. The process could also lead to formation of ungrafted polymer suspended in the reaction solution, which may deplete free monomers for surface grafting and may clog the microfluidic channels.¹⁴ Solutions to reduce hydrophobicity include activation of the polymer surface by hydrophilizing treatments, such as plasma,^{15,16} UV/ozone,^{17,18} and corona discharge treatment.¹⁹ Drawbacks of such treatments may include polymer surface damage or treatment degradation during time of usage.²⁰

SiO₂ thin films have been broadly used in integrated circuits (ICs) and microfabrication techniques.²¹ They can serve as the insulating material to block the interconnection between two devices; or they can provide chemical functional groups or linkers to bind a plethora of compounds to the substrate surface. In addition, their hydrophilic characteristics in aqueous solutions can significantly mitigate surface problems of polymers in chemical and biological sensing applications. It was reasoned that by depositing an SiO₂ thin film on the surface of COC structures, the hybrid will take advantage of both materials: the unique properties and fast and inexpensive prototyping capability of COC,

and the well established surface chemistry of SiO₂ thin films. In addition, SiO₂ thin films are less likely to affect the optical properties of COC.

In the current report we describe a method of depositing SiO₂ thin films on a COC surface using a low-temperature sputtering technique. We further describe the characterization of the deposited SiO₂ thin film and the physical, optical, and chemical properties of the SiO₂-COC hybrid material. Finally, we show that this method and the resulting hybrid material are well suited for microfabrication purposes and for subsequent surface functionalizations.

2. Experimental

All chemicals were purchased and used as received without further purification. Acetone, isopropyl alcohol (IPA), ethanol, methanol, methylene chloride, tetrahydrofuran (THF), and acetonitrile (ACN) were purchased from VWR. Hydrochloric acid, sulfuric acid, sodium hydroxide, NH₄OH, phosphate buffered saline solution, Tris-EDTA buffer were purchased from Sigma and diluted with dI H₂O.

COC plates (Topas 6015, 6'' × 6'') were purchased from Topas (Florence, KY). A plate was cut into small pieces with desired dimensions to fit into different characterization tools. Samples were cleaned in a clean-room environment by the RCA method (NH₄OH-H₂O₂-dIH₂O = 1 : 1 : 5) at 80 °C for 15 min and dried by a stream of nitrogen. Samples were baked in a vacuum oven at 110 °C for 1 h before film deposition.

Silicon dioxide films were deposited by using a Kurt Lesker PVD 75 (Kurt J. Lesker Company, Pittsburgh, PA) RF magnetron sputtering system. A 3'' SiO₂ sputtering target (99.995% purity) was used. Substrates were fixed on a holder on top of the target and the holder rotated at constant speed for uniform deposition. The chamber was pumped down to 5.0 × 10⁻⁶ Torr and gases were purged into chamber by opening the gas valve. High-purity Ar and O₂ were mixed by pre-set program "MODE 2" and were introduced to the chamber to reach the desired gas pressure and stabilize. RF power was gradually increased to the desired level with the shutter closed at a ramp rate of 10 W min⁻¹. The shutter was opened at the desired RF power level and deposition was timed.

The deposited film thickness was measured with an optical interferometer, Nanometrics 210 (Nanometrics Incorporated, CA). A 10× objective lens for small spot size focus and the standard "Oxide on Silicon" thickness measurement program were employed. A total of five points for each sample were randomly chosen for measurement. The average deposition rate was calculated by dividing the total film thickness by the total deposition time. Due to the close refractive indices between SiO₂ film and the COC substrate, and the fact that both layers are transparent, the film thickness could not be directly measured by most optical techniques. Therefore, a small piece of silicon wafer was put into the deposition chamber along with the COC substrate for total film thickness measurements.

Infrared absorption spectra were collected on a Thermo Electron Nicolet 8700 FTIR spectrometer equipped with the Vectra-Piezo™ interferometer. A smart Orbit ATR module accessory with a Ge crystal as an internal reflection element was used. For background and sample, 32 scans at 2 cm⁻¹ resolution were collected.

Chemical binding energy analyses of the film were performed using a Kratos Analytical Axis Ultra X-ray photoelectron spectrometer (Kratos Analytical Inc, New York) with a monochromatic Al KR X-ray source radiation at 1486.6 eV. The survey spectrum was an average of ten sweeps at pass energy of 160 eV, 1 eV per step resolution and 200 ms dwell time. For high-resolution regions spectra of C1s, O1s, and Si1 p were an average of ten sweeps at pass energy of 20 eV, 1 eV per step resolution and 200 ms dwell time.

UV-vis spectra were collected on a Shimadzu UV-3600. The transmittance percentage was measured from 250 to 700 nm with sampling interval of 1 nm. Slit width was 2 nm and each sample was single scan. The resulting spectra were analyzed and reported by the software UVProbe™.

Atomic force microscope images were collected in tapping mode using a Digital Instruments Dimension 3100 produced by Veeco Instruments Inc. (Plainview, NY). 3-aminopropyl triethoxy silane (APTES) was used to functionalize the COC-SiO₂ surface. The silanes were dissolved at 1% (v/v) concentration in a solvent of 95% methanol and 5% dIH₂O. Samples were incubated in the solution at room temperature for 15 h. The samples were washed with original solvent and dried with a nitrogen stream. The samples were then baked in an oven at 120 °C for 2 h.

3. Results and discussion

3.1. Fabrication of SiO₂-COC hybrid

In order to select a suitable method for binding SiO₂ thin film on COC, we evaluated potential deposition methods, including chemical vapor deposition (CVD)²² and physical vapor deposition (PVD).²³ In CVD, the reactants are absorbed on the hot substrate surface where film-forming reaction occurs. Since the substrate must be heated to a high temperature (typically higher than 300 °C), this approach is not practical for COC. PVD can be done at lower temperatures and therefore maybe suitable. In PVD, we preferred sputtering over evaporation due to excellent film adhesion, improved film uniformity control, and step coverage.²⁴ Apart from surface self-heating by target atom energy dissipation, sputtering is considered a low-temperature process. Nowadays, sputtering techniques have been broadly employed in applying films to computer disks, compact discs (CDs), liquid crystal displays, and so on. Therefore, we decided to test sputtering for deposition of SiO₂ thin film onto COC.

The deposition rate was the first parameter to be tuned in order to control the thickness of thin film deposition. In a sputtering system, the film deposition rate is influenced by the anode-to-cathode distance, gas pressure, and RF

power. Since the anode-to-cathode distance was kept constant in this study, only the gas pressure and the power were adjusted. As shown in Fig. 1, decreasing gas pressure or increasing power will increase the deposition rate. This can be explained by the kinetic molecular theory, which states that the mean-free-path of a sputtered atom is inversely proportional to the total gas pressure in the chamber.²⁵ In our study, a maximum rate of 16.5 nm per min was achieved at a setting of 300 W and 5 mTorr.

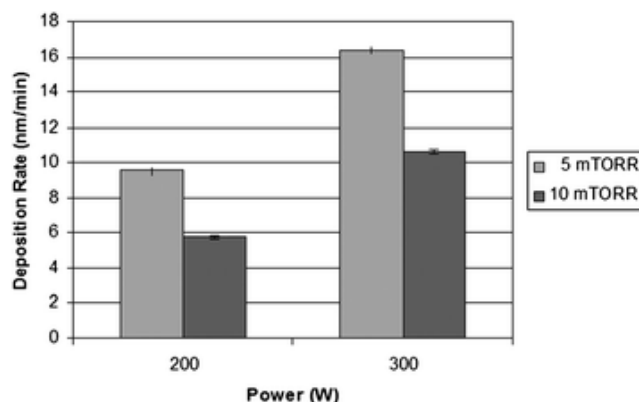


Fig. 1 Deposition rates of SiO₂ thin film at different sputtering powers and pressures.

3.2. Characterization of the deposited thin film

To investigate the chemical bonding structure of the deposited thin film, we used Fourier transform infrared spectroscopy (FTIR). The spectra were recorded using a Thermo Electron Nicolet 8700 FTIR spectrometer. An attenuated total reflection (ATR) sampling module with Smart Orbit accessory and a germanium crystal plate were utilized to analyze the thin oxide film on the substrate. The measurements were taken over wave numbers ranging from 4000 cm⁻¹ to 500 cm⁻¹ at a resolution of 2 cm⁻¹. It was acknowledged that the optical setups were different in the ATR and the transmission experiments. Thus, when comparing the transmissions, the relative peaks in the ATR spectrum showed distortions in relative intensities and shifted to lower frequencies. To eliminate these distortions, a correction algorithm introduced in software package OMNIC™ 6.2 (Thermo Scientific Nicolet™) was applied to all obtained spectra. The corrected spectra of different ATR samples are shown in Fig. 2. The spectrum of the sample with RF sputtered thin film shows two intense bands at 809 cm⁻¹ and 1071 cm⁻¹, corresponding to the Si–O–Si bending and stretching modes, respectively (Fig. 2b), which have been reported in the literature.^{26,27} However, since the lower detection wave number limit was determined by the internal reflection element (IRE) and that the limit of the IRE used in our system was approximately 600 cm⁻¹ (Ge),²⁸ the third band corresponding to the rocking modes (ω_1) at approximately 450 cm⁻¹ was out of range in our spectrum. The two absorption bands at 1196 cm⁻¹ and 1071 cm⁻¹ were both assigned to the asymmetric Si–O–Si vibration mode, where oxygen atoms move back and forth along the axis line of the silicon atoms. By comparison, these bands did not appear in the spectrum of the untreated COC sample (Fig. 2a). In both spectra, the absorption at 2950 cm⁻¹ – 2850 cm⁻¹ region was assigned to the carbon/hydrogen stretching vibration modes of –CH₂ and –CH₃. Additionally, the peak around 1453 cm⁻¹ represents the wagging mode of –CH₃ in the polymer backbone. These peaks were significantly smaller in Fig. 2b, which indicated the covering of the polymer surface. The broad absorption peak around 3400 cm⁻¹ in Fig. 2b was assigned to the hydroxyl group stretching, which was related to the presence of Si–OH vibration. It is believed that the –OH group on deposited SiO₂ film is formed by interaction between SiO₂ and moisture in ambient air.²⁹ This band was absent in the spectrum of untreated sample (Fig. 2a), which further indicated successful deposition of the SiO₂ film.

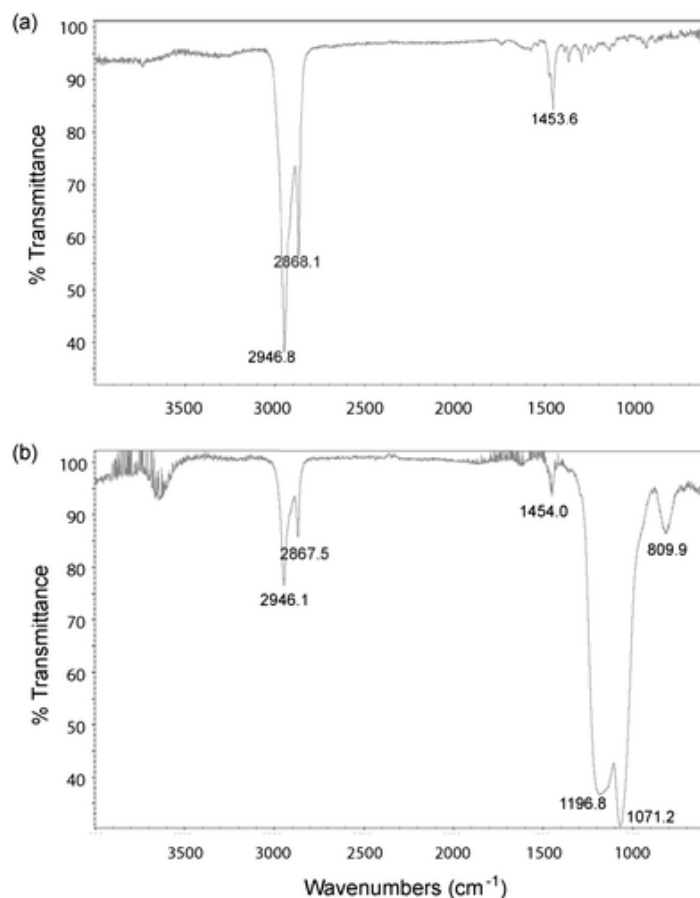


Fig. 2 Infrared spectra of COC samples. (a) Without SiO₂ deposition. (b) With SiO₂ deposition.

X-Ray photoelectron spectroscopy (XPS) analysis was used to further characterize the sputtered SiO₂ on the COC surface (Fig. 3). A representative survey spectra collected from untreated COC indicated typical C(1s) peak (284.5 eV), O(1s) peak (529.5 eV) and O KLL peaks (973.5 eV) (Fig. 3a). The survey spectra of SiO₂ sputtered COC showed dramatic increase in O(1s) intensity and equally dramatic decrease in C(1s) intensity (Fig. 3b). In addition, the two prominent peaks at 153.6 eV (Si 2s) and 102.6 eV (Si 2p) agreed well with the reported binding energies of SiO₂,³⁰ which further confirmed the presence of SiO₂ film on the polymer surface (Fig. 3b). Concentrations of carbon, oxygen and silicon atoms on both sample surfaces were estimated from peak areas. Ratios of oxygen-to-carbon (O/C) and silicon-to-carbon (Si/C) were calculated using atomic percentage in spectra and the results for both samples are listed in Table 1. Comparing the modified with the bare surface, the average O/C ratios changed from 0.047 to 8.68, while the average Si/C ratios for 0 to 3.86. This result was consistent with the expected surface modification. A reduction in C(1s) intensity was expected when the surface was coated by SiO₂. In addition, the incorporation of oxygen and silicon atoms was also expected to increase the ratios of O/C and Si/C. The high ratios of O/C and Si/C on coated sample demonstrated the high efficiency of the sputtering process.

Table 1 XPS compositional analysis of COC samples with and without SiO₂ film deposition.^a

| | Atomic concentration (%) | | | | |
|----------------------|--------------------------|----------------|-----------------|--------------------------------|---------------------------------|
| | X _C | X _O | X _{Si} | X _O /X _C | X _{Si} /X _C |
| COC | 95.52 | 4.48 | — ^a | 0.0469 | — ^a |
| COC/SiO ₂ | 7.38 | 64.09 | 28.53 | 8.6842 | 3.8658 |

^a Element not present.

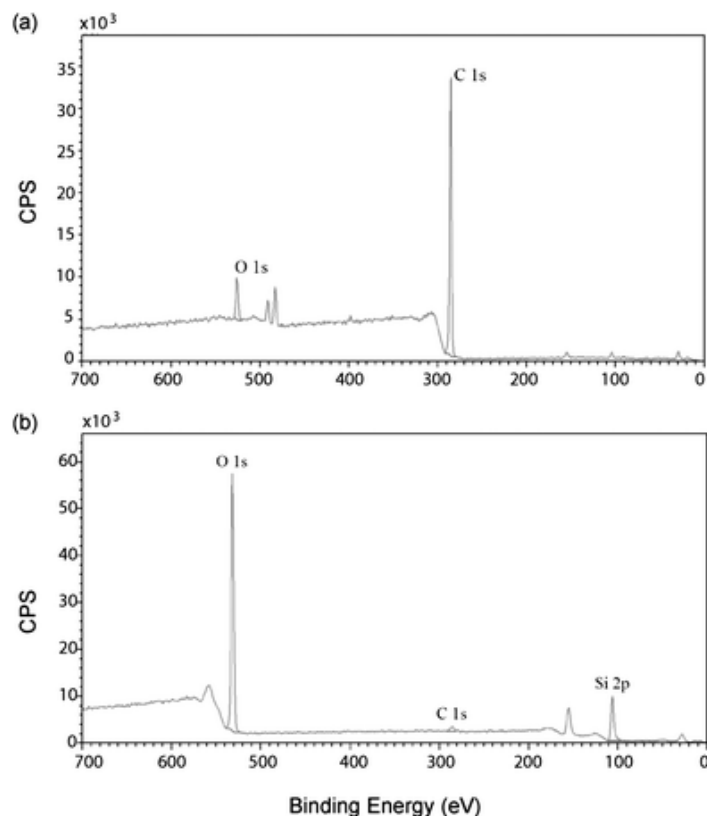


Fig. 3 XPS survey scans of COC samples. (a) Without SiO₂ deposition. (b) With SiO₂ deposition. A take-off angle (t.o.a.) of 90° was used for all XPS measurements in this study.

The surface wettability change after SiO₂ deposition was characterized by water contact angle measurements using a NRL CA Goniometer (Ramé-Hart, NJ, USA). The contact angle of the water drop was 100.5° on the COC surface before silica film deposition. After film deposition, the contact angle decreased to 17°. The dramatic surface wettability change was clearly caused by the SiO₂ film deposition.

3.3. Characterization of SiO₂-COC hybrid

3.3.1. Optical transmission. It has been known that COC shows significant light transparency in near-UV and visible light regions of the electromagnetic spectrum. The optical loss for COC in the visible range is less than 1 dB-cm⁻¹.³¹ To investigate whether the ionic bombardment and substrate surface heating during the film deposition process damaged the optical transmission properties of the polymer, we measured a COC sample before and after film depositions using a UV-vis spectrophotometer. The optical transmission spectra of COC and oxCOC were taken at normal light incident under the ambient conditions. As shown in Fig. 4, the transmittance of the hybrid sample was close to 90% from 700 nm to 400 nm; it gradually decreased to around 70% at 360 nm and quickly dropped to zero when the wavelength approaches 250 nm. The UV-vis spectrum of the hybrid was almost identical to that of the non-functionalized COC substrate in the full measured range, which indicated that the sputtering deposition did not cause polymer surface damage or material deformation by either ionic bombardment or surface heating. Furthermore, the high transmission (>80%) characteristic of the hybrid material in the near UV range (>350 nm) implied that this coating technique can be applied to the optical COC devices in different applications, which require surface coating with hybrid materials for light irradiation without sacrificing the high transmission characteristics.

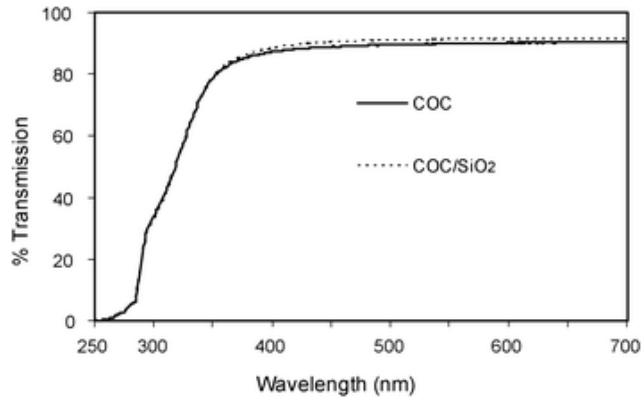


Fig. 4 UV-vis spectroscopy transmission measurements of COC samples before and after SiO₂ film deposition.

3.3.2. Surface morphology and roughness. The mean surface roughness (R_a) and root-mean-square roughness (R_q) of SiO₂ coated and uncoated COC samples were measured with a profilometer and atomic force microscope (AFM). The profilometer was used to measure the roughness of a big surface area (500 μm linear range) and the AFM was used to scan a small surface area (2 $\mu\text{m} \times 2 \mu\text{m}$). Two samples were used for profilometer measurements. Six points were randomly chosen on the surface of each sample before and after film deposition. The roughness were calculated from the surface profile images and averaged. For AFM imaging, the tapping mode was used. In survey scans, areas of 25 μm^2 (5 $\mu\text{m} \times 5 \mu\text{m}$) were first imaged at low resolution (128 lines per sample); a 4 μm^2 (2 $\mu\text{m} \times 2 \mu\text{m}$) area was then chosen and re-scanned at higher resolution (256 lines per sample). After scan capture, images were flattened by first-order X - Y plane-fitting. The roughness was determined by the capture and flattening software. The roughness data on both coated and uncoated samples are listed in [Table 2](#). The three dimensional AFM images are shown in [Fig. 5](#). Data in [Table 2](#) indicates that the deposition caused very slight increase in roughness on the surface.

Table 2 Surface roughness (R_a , R_q) of COC samples with and without SiO₂ film deposition as measured by profilometer (wide range) and AFM (narrow range)

| | Profilometer | | AFM | |
|----------------------|----------------|-----------------|-----------------|-----------------|
| | R_a | R_q | R_a | R_q |
| COC | 8.63 \pm 1.6 | 10.88 \pm 2.1 | 3.44 \pm 0.84 | 4.32 \pm 0.74 |
| COC/SiO ₂ | 9.60 \pm 2.0 | 12.00 \pm 2.5 | 3.75 \pm 0.53 | 4.79 \pm 0.61 |

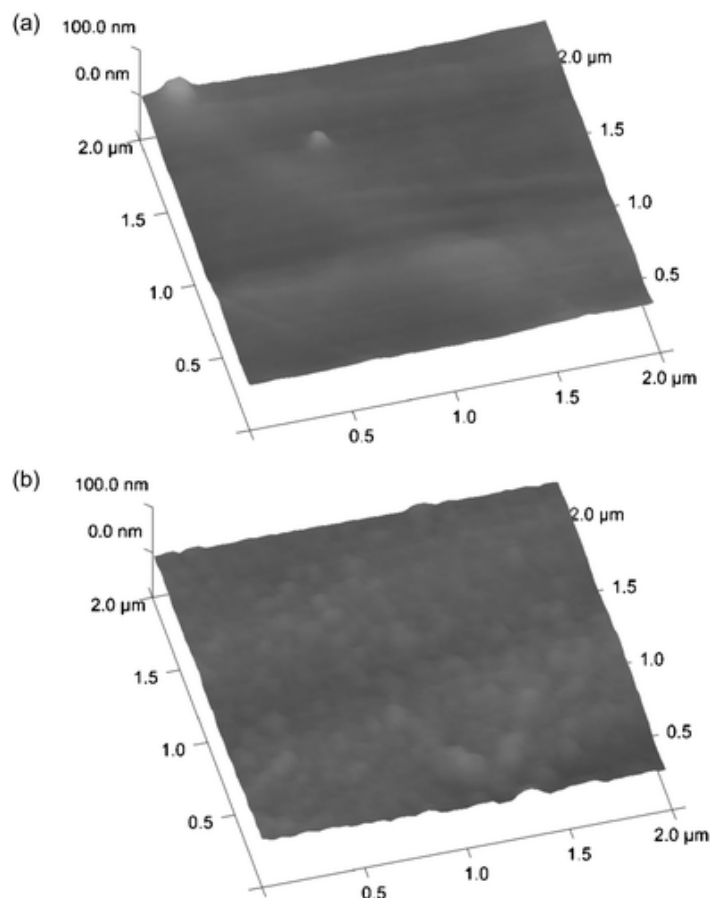


Fig. 5 AFM scan images of COC surfaces. (a) Without sputtered SiO₂ film. (b) With sputtered SiO₂ film.

The surface thin film roughness is strongly related to the deposition mechanism, which is controlled by the mobility of atoms on the surface. The increase in atom mobility will result in lower roughness. During sputtering deposition, the atom mobility can be enhanced by using higher power to bombard the target atoms. In our study, although we did not compare roughness of different samples made by different deposition powers, the sample we studied was made at a power level of 300 W, which provided enough energy to the atoms to produce a smooth coating surface. On the other hand, higher power produced a higher-energy dispersion of deposited atoms and caused the substrate to self-heat. If the heating temperature became higher than the T_g , the plastic substrate would deform and increase surface roughness. In our study, although the substrate temperature increased during the deposition, we did not observe any significant damage or increase in roughness of the substrate surface.

3.4. Chemical and mechanical stability of SiO₂-COC hybrid

Solvent or chemical compatibility is one of the most important parameters in determining the adequacy of a surface coating technique. To investigate whether sputtered SiO₂ on COC can be employed in different applications, the coated samples were immersed in fourteen different solvents separately for 24 h. The solvents being tested included water, phosphate buffered saline (PBS, 1X), Tris-EDTA buffer (TE, 1X), hydrochloric acid (1 M), sulfuric acid (2 M), sodium hydroxide (1 M), NH₄OH (27%), acetone, isopropyl alcohol (IPA), ethanol, methanol, methylene chloride, tetrahydrofuran (THF), and acetonitrile (ACN). Following incubation, samples were rinsed by deionized water and dried by nitrogen gas. Each sample was first inspected visually for any morphology changes, such as swelling and bleaching. ATR-FTIR was then used to investigate the variation in Si-O adsorption ([Fig. 6](#)).

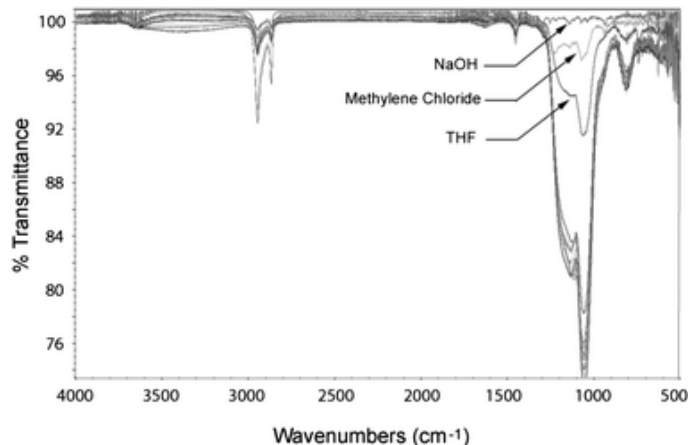


Fig. 6 ATR FT-IR analyses of COC–SiO₂ samples after chemical or solvent treatments.

As summarized in [Table 3](#), there were no obvious changes in morphology for samples in water, PBS buffer, TE buffer, acidic aqueous solutions as well as polar organic solvent such as acetone, IPA, ethanol, or methanol. No obvious damage was observed on the SiO₂ film or the COC substrate in ACN. In basic aqueous solutions, the sample in NH₄OH showed no damage on either the SiO₂ film or the COC substrate. Correspondingly, there was little change in the ATR FT-IR spectra for these samples ([Fig. 6](#)). However, the SiO₂ film was stripped from the COC surface when immersed in 1 M NaOH solution as indicated by the disappearance of the two absorption bands at 1196 cm⁻¹ and 1071 cm⁻¹, which were assigned to the asymmetric Si–O–Si vibration mode ([Fig. 6](#)), although there was no surface damage to the COC substrate. Severe damages to the SiO₂ film were observed in methylene chloride and THF as evident by significant decreases of the two bands. Damages to both samples might be attributed to the COC swelling and deformation in the solvents.

Table 3 Chemical compatibility of SiO₂–COC hybrid

| | No damage | Film damage ^a | Both damage |
|--------------------------------------|-----------|--------------------------|-------------|
| H ₂ O | ✓ | | |
| PBS, 1X | ✓ | | |
| TE, 1X | ✓ | | |
| HCl, 1 M | ✓ | | |
| H ₂ SO ₄ , 2 M | ✓ | | |
| NaOH, 1 M | | ✓ | |
| NH ₄ OH, 27% | ✓ | | |
| Acetone | ✓ | | |
| IPA | ✓ | | |
| Ethanol | ✓ | | |
| Methanol | ✓ | | |
| Methylene chloride | | | ✓ |
| THF | | | ✓ |
| Acetonitrile | ✓ | | |

^a With no damage to substrate.

The mechanical stability of the SiO₂–COC hybrid was investigated by sonication, a treatment often used in surface cleaning. It was found that the SiO₂–COC hybrid remained intact after over 10 min of sonication at maximum power setting of 10 in a Crest Tru-Sweep Genesis Ultrasonic Cleaner (Crest Ultrasonics, Trenton, NJ). According to the above experimental studies, we believe that although there is no covalent bond formed between COC and the SiO₂ coating, the silica film can strongly attach to COC and the adhesion strength is sufficient for most MEMS processes.

3.5. Surface functionalization of oxCOC with amino-silane

To assess whether the oxCOC surface is suitable for further modification by other compounds, we did a test using APTES molecule. The procedure to link APTES onto COC surface is shown in [Fig. 7a](#). XPS analyses of functionalized

surface confirmed changes in surface composition (Fig. 7b). Analysis of survey spectra showed the appearance of a peak with binding energy of 399 eV. This peak was assigned to nitrogen atom N(1s) bound to hydrogen (N–H group), which was consistent with literature.³² Other peaks at 532, 284, and 102 eV were assigned to O(1s), C(1s) and Si(2p), respectively. The peak at 284 eV increased significantly after silanization. This peak represented carbon atoms bound to hydrogen (C–H groups), which were found in the Si–CH₃ and –CH₂– groups of the silane molecule. Similarly, ATR FT-IR analysis of the COC–SiO₂ surface before (Fig. 7c) and after APTES conjugation (Fig. 7d) showed the appearance of two broad peaks indicative of presence of amine function groups on oxCOC surface. The peak around 3650 ~ 3300 cm⁻¹ was assigned to N–H stretch and the peak at 1695 cm⁻¹ was assigned to N–H bending. Therefore, both the XPS and the ATR FT-IR analyses demonstrated successful functionalization of the silica film surface with APTES.

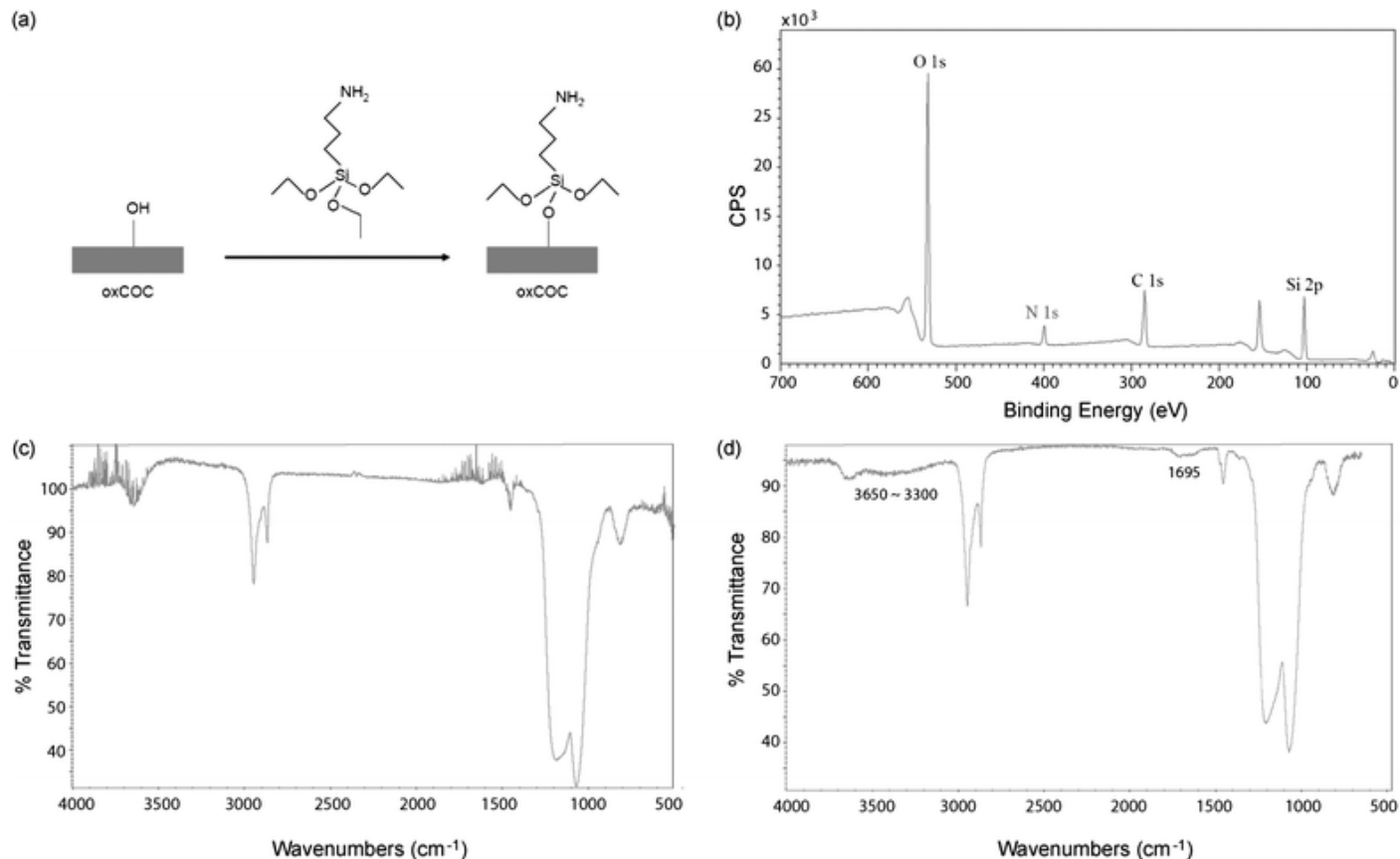


Fig. 7 Surface modification of oxCOC by APTES. (a) Schematic illustration of the chemistry used for surface modification. (b) XPS survey scans of APTES silanized oxCOC surface. The N(1s) peak demonstrates successful functionalization. (c) ATR FT-IR spectroscopy of the silica film before functionalization with APTES. (d) ATR FT-IR spectroscopy of the silica film after functionalization with APTES.

4. Conclusions

In this study, we developed a robust and efficient process of depositing an SiO₂ thin film on a COC surface at low temperature using RF sputtering technique. Since there is no high temperature requirement in the process, this technique can be applied to COC materials of different T_g and potentially to other polymers as well. Characterization of the SiO₂–COC hybrid material revealed desirable physical, optical and chemical properties ideal for a variety of potential BioMEMS applications. We believe that the SiO₂–COC hybrid material will be highly suitable for fabrication of microfluidic and lab-on-a-chip devices because it combines the desirable properties of both COC and silicon dioxide. It allows rapid and inexpensive prototyping and fabrication as COC does. The well characterized surface chemistry and functionalization techniques developed for silica substrates can be readily applied to the SiO₂–COC hybrid materials.

Acknowledgements

We thank Dr Mark Walters for helpful discussions. J. T. is a Beckman Young Investigator and a recipient of a Hartwell Individual Biomedical Research Award.

References

- 1 R. R. Lamonte and D. McNally, *Plast. Eng.*, 2000, **56**, 51.
- 2 R. R. Lamonte and D. McNally, *Adv. Mater. Process.*, 2001, **159**, 33–36.
- 3 M. B. Hochrein, C. Reich, B. Krause, J. O. Radler and B. Nickel, *Langmuir*, 2006, **22**, 538–545 [[Links](#)].
- 4 H. D. Bauer, W. Ehrfeld, J. Hossfeld and T. Paatzsch, *Opt. Fabrication Testing*, 1999, **3739**, 224–229.
- 5 H. D. Bauer, W. Ehrfeld, M. Harder, T. Paatzsch, M. Popp and I. Smaglinski, *Synth. Met.*, 2000, **115**, 13–20.
- 6 C. Li, Y. N. Yang, H. G. Craighead and K. H. Lee, *Electrophoresis*, 2005, **26**, 1800–1806 [[Links](#)].
- 7 D. Nilsson, S. Balslev and A. Kristensen, *J. Micromech. Microeng.*, 2005, **15**, 296–300 [[Links](#)].
- 8 D. S. Kim, S. H. Lee, C. H. Ahn, J. Y. Lee and T. H. Kwon, *Lab Chip*, 2006, **6**, 794–802 [[Links](#)].
- 9 D. A. Mair, E. Geiger, A. P. Pisano, J. M. J. Frechet and F. Svec, *Lab Chip*, 2006, **6**, 1346–1354 [[Links](#)].
- 10 J. Steigert, S. Haerberle, T. Brenner, C. Muller, C. P. Steinert, P. Koltay, N. Gottschlich, H. Reinecke, J. Ruhe, R. Zengerle and J. Ducree, *J. Micromech. Microeng.*, 2007, **17**, 333–341 [[Links](#)].
- 11 M. F. Bedair and R. D. Oleschuk, *Anal. Chem.*, 2006, **78**, 1130–1138 [[Links](#)].
- 12 Q. S. Pu, O. Oyesanya, B. Thompson, S. T. Liu and J. C. Alvarez, *Langmuir*, 2007, **23**, 1577–1583 [[Links](#)].
- 13 T. Rohr, D. F. Ogletree, F. Svec and J. M. J. Frechet, *Adv. Funct. Mater.*, 2003, **13**, 264–270 [[Links](#)].
- 14 S. W. Hu, X. Q. Ren, M. Bachman, C. E. Sims, G. P. Li and N. L. Allbritton, *Anal. Chem.*, 2004, **76**, 1865–1870 [[Links](#)].
- 15 D. Nikolova, E. Dayss, G. Leps and A. Wutzler, *Surf. Interface Anal.*, 2004, **36**, 689–693 [[Links](#)].
- 16 S. Laib and B. D. MacCraith, *Anal. Chem.*, 2007, **79**, 6264–6270 [[Links](#)].
- 17 G. A. Diaz-Quijada, R. Peytavi, A. Nantel, E. Roy, M. G. Bergeron, M. M. Dumoulin and T. Veres, *Lab Chip*, 2007, **7**, 856–862 [[Links](#)].
- 18 C. W. Tsao, L. Hromada, J. Liu, P. Kumar and D. L. DeVoe, *Lab Chip*, 2007, **7**, 499–505 [[Links](#)].
- 19 Q. C. Sun, D. D. Zhang and L. C. Wadsworth, *Tappi J.*, 1998, **81**, 177–183.
- 20 J. Gaudioso and H. G. Craighead, *J. Chromatogr., A*, 2002, **971**, 249–253 [[Links](#)].
- 21 D. A. Buchanan, *IBM J. Res. Dev.*, 1999, **43**, 245–264 [[Links](#)].
- 22 S. Taylor, J. F. Zhang and W. Eccleston, *Semicond. Sci. Technol.*, 1993, **8**, 1426–1433.
- 23 R. F. Bunshah and C. V. Deshpandey, *J. Vac. Sci. Technol., A*, 1985, **3**, 553–560.
- 24 S. Schiller, K. Goedicke, J. Reschke, V. Kirchhoff, S. Schneider and F. Milde, Elsevier Science, Lausanne, 1993, pp. 331–337.
- 25 J. H. Keller and R. G. Simmons, *IBM J. Res. Dev.*, 1979, **23**, 24–32.
- 26 W. A. Pliskin and H. S. Lehman, *J. Electrochem. Soc.*, 1965, **112**, 1013 [[Links](#)].
- 27 G. Lucovsky, M. J. Manitini, J. K. Srivastava and E. A. Irene, *J. Vac. Sci. Technol., B*, 1987, **5**, 530–537.
- 28 H. Hosono, *J. Appl. Phys.*, 1991, **69**, 8079–8082.
- 29 C. C. Perry and X. C. Li, *J. Chem. Soc., Faraday Trans.*, 1991, **87**, 761–766 [[Links](#)].
- 30 W. J. Coleman, *Appl. Opt.*, 1974, **13**, 946–951.
- 31 G. Khanarian and H. Celanese, *Opt. Eng.*, 2001, **40**, 1024–1029.
- 32 A. A. Vaidya and M. L. Norton, *Langmuir*, 2004, **20**, 11100–11107 [[Links](#)].